Supplement of Atmos. Chem. Phys., 25, 10075–10087, 2025
https://doi.org/10.5194/acp-25-10075-2025-supplement

Atmospheric Chemistry and Physics
Open Access

Supplement of

Measurement report: Aerosol and cloud nuclei properties along the Central and Northern Great Barrier Reef – impact of continental emissions

E. Johanna Horchler et al.

Correspondence to: E. Johanna Horchler (eva.horchler@qut.edu.au)

S1. Details on the instrumental set-up and data analysis

Particle number concentration (> 7 nm) and size distribution were obtained using a Mixing Condensation Particle Counter (mCPC 1720, Brechtel Manufacturing Inc.), a Scanning Electrical Mobility Spectrometer (SEMS 2100, Brechtel Manufacturing Inc.) combined with a mCPC 1720, and an Aerodynamic Particle Sizer (APS 3321, TSI Inc.). The SEMS was operated at a sheath flow rate of 5 L min^{-1} and set to scan 150 aerosol diameter bins from 5 to 1081 nm, in both up and down scanning modes, with a 5-minute scan time. The APS captured size distributions from 0.5 to 5 µm, with a time resolution of 2 minutes. The APS data was exported with Stokes correction turned on and an assumed density of 1.3 g cm^{-3}. The density was chosen under the assumption that the particles are composed of sea salt and an inlet relative humidity of approximately 50 %. APS measurements for particle diameters less than 700 nm were removed due to known measurement biases at these diameters (Beddows et al., 2010). APS aerodynamic diameters were converted to the volume equivalent diameter (DeCarlo et al., 2004). The particle density required for the conversion was modelled as a function of relative humidity using E-AIM (Wexler and Clegg, 2002) and an assumed particle composition of NaCl with 1.3 g cm^{-3} at 50 % RH. The APS and SEMS diameters were further corrected for the relative humidity dependent growth factor (GF), which is computed taking the measured RH by the SEMS, and assuming a composition of ammonium sulfate for the SEMS and sea salt for the APS based on the size-dependent chemical composition typically observed in marine sea spray aerosols (Heintzenberg et al., 2000). In the absence of RH data, an RH of 48 % was estimated as the average value across the entire period. The APS and SEMS data were corrected for size-dependent inlet losses (Fig. S1), combined into a single size distribution ranging from 5 nm to 5000 nm and re-binned onto a 32-channel per decade set of particle diameters. Overlapping bins were averaged. Due to instrument artifacts, concentrations for particles smaller than 10 nm were not reliable and thus were not considered.

The CCN-100 measured the total CCN number concentration at a range of supersaturations (0.1 %, 0.2 %, 0.3 %, 0.5 %, 0.7 % for 10 minutes each). The data are processed to remove the first 150 seconds of data at supersaturations 0.2 to 0.7 % and 300 seconds at 0.1 %

supersaturation to ensure that the supersaturation has stabilised in the instrument. The κ-Köhler model was used to determine the hygroscopicity parameter for the background aerosol (Petters and Kreidenweis, 2007). Therefore, the critical diameter for cloud droplet activation was determined by integrating the size distribution, from the largest diameter to the diameter at which the integration is equal to the measured CCN number concentration at the measured supersaturation. For this calculation, a size-independent homogeneous aerosol composition and internal particle mixing were assumed. This is presumably only valid for background aerosols, while in most cases aerosols of different size have different composition and are not necessarily internally mixed. The uncertainties associated with this method could result in an incorrect estimation of the critical diameter (D_{crit}) and thus also of the required SS for CCN activation. The measured CCN was taken as the average of the CCN measured during the averaging period for the size distribution. The measurement uncertainty in the computed critical diameter was computed as a sum of the standard deviation in the mean of the CCN number concentrations and the relative uncertainty in the size distribution. The size distribution uncertainty was assumed to be equal to the standard deviation in the mean of the CPC concentrations over the averaging period, which assumes that the uncertainty in the distribution is not dependent on particle diameter. The hygroscopicity parameter was then computed for the above calculated critical diameter (Petters and Kreidenweis, 2007). The Hoppel Minimum, which is formed due to the in-cloud growth of aerosol, was calculated as the global minimum between 30 nm and

150 nm if present. The corresponding effective maximum in-cloud supersaturation at the Hoppel minimum can be approximated via κ -Köhler theory using the hygroscopicity parameter κ (Gong et al., 2023).

The time zone was set to UTC time for all measurements. The times were adjusted for time delays between the individual instruments. For comparison reasons, all instruments, except the SEMS were averaged onto the same timescale of one hour unless stated otherwise.

NOAA's Hybrid-Single-Particle Lagrangian Integrated Trajectory (HYSPLIT) dispersion model (Stein et al., 2015) was used to calculate back trajectories, representing the path taken by each air mass during the three days prior to reaching the ship. Because air masses that passed over land within three days before reaching the ship showed a clear land signature, but associated HYSPLIT back-trajectory errors are proportional to 15 to 30 % of the trajectory travel distance (Draxler and Rolph, 2007), the back-trajectory duration was thus limited to three days. The dispersion model was underpinned by meteorological data obtained from the Global Data Assimilation System (GDAS) dataset at 1° spatial resolution. To ensure that the trajectory starting height is representative of the airmass pathways, starting heights of 0.5 of the planetary boundary layer (PBL) height, and 10 m above mean sea level, which corresponds to the sampling inlet height, were evaluated. Because both approaches yield similar trajectories, a starting height of 10 m above sea level was chosen to account for the actual sampling height and allow for greater variations in the vertical dimension within the PBL. This is required for the calculation of HYSPLIT ensemble trajectories, which apply small spatial perturbations based on user-defined grid offsets to the end point prior to estimating the trajectories. In this study for each hour of sampling, an ensemble of 27 trajectories was generated. Each ensemble was then averaged to give a trajectory that best represented the path taken by the air mass. To identify periods that may have been influenced by continental emissions, continental boundaries were sourced from the ArcGIS Hub (Esri, 2021). Any air masses that passed over land within three days of reaching the ship were classified as "continental".

Figure S1: (a) Exterior of the Cloud-Cube (b) data logging, inlet control systems, UHSAS, filter sampler, airconditioner (c) APS, SEMS, TAP, CPC's and CCNc.

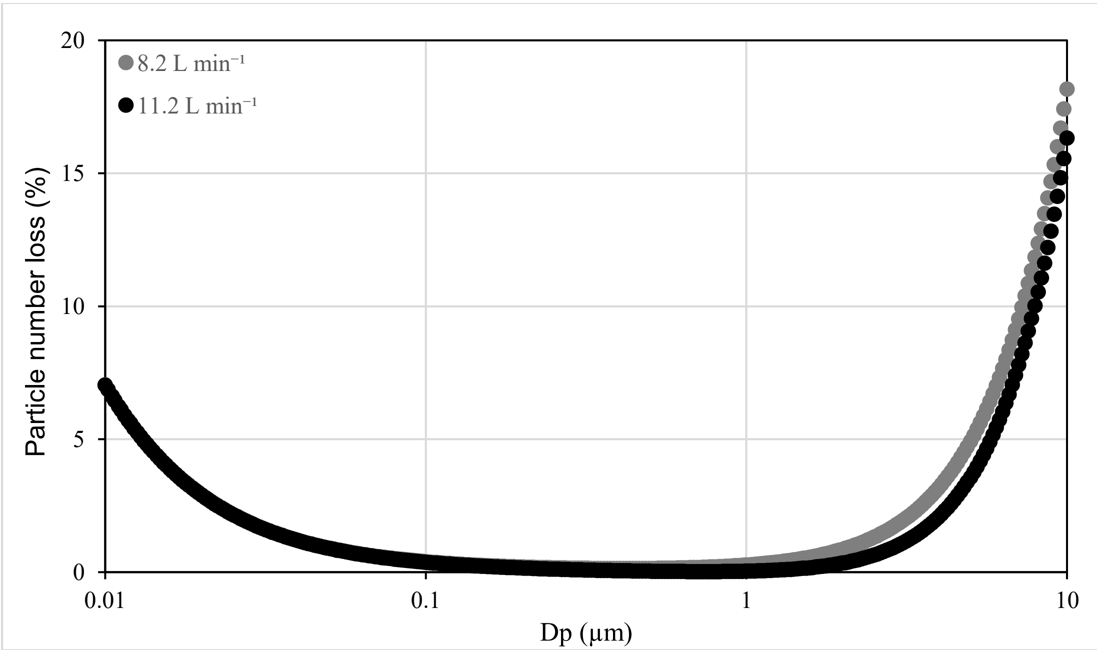

Figure S2: Particle number loss as a function of diameter for the aerosol sampling equipment during the Atmospheric Survey in February and March 2022 as modelled using the Particle Loss Calculator. All instruments running together made up a total flow rate of 11.2 L min^{-1}. In the case where the filter sampler was not running, the total flow rate was 8.2 L min^{-1}. The corresponding particle loss correction was applied for each flow rate, even though differences in the particle losses are only significant for supermicron particles.

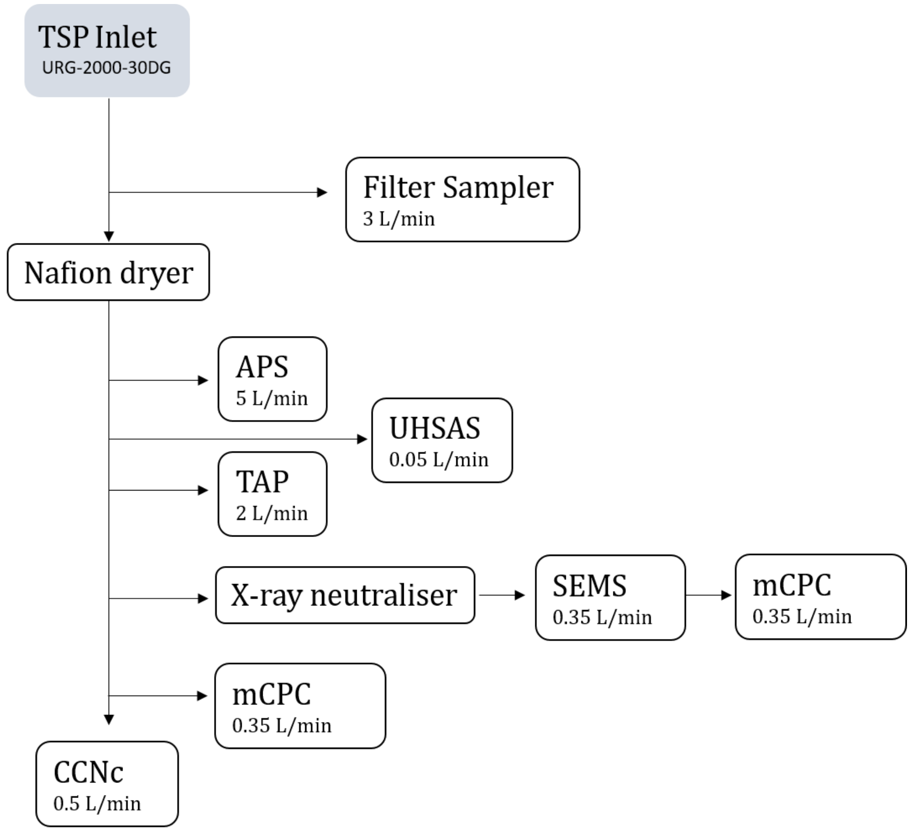

Figure S3: Schematic of the set-up. Arrows indicate the flow directions.

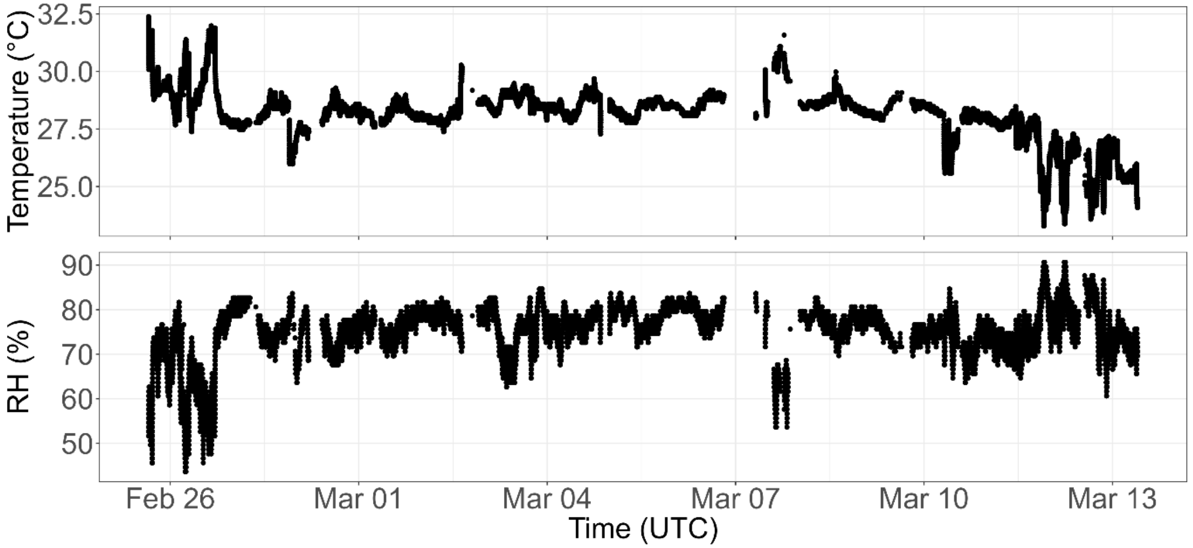

Figure S4: Time series of the temperature and RH.

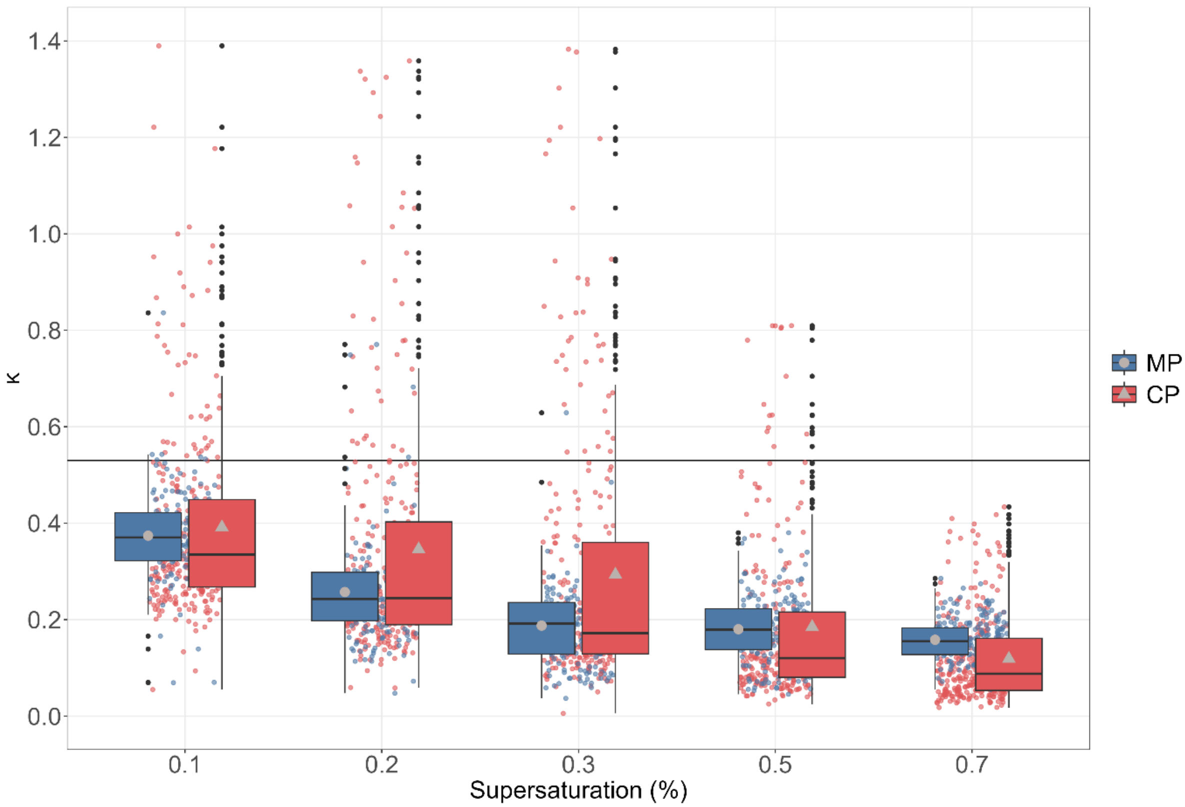

Figure S5: Aerosol hygroscopicity parameters κ for the MP (blue) and CP (red) averaged on a minute timeframe at different supersaturations. The black horizontal line at 0.53 indicates the hygroscopicity parameter κ for pure ammonium sulfate (Petters and Kreidenweis, 2007). The black horizontal line in a box displays the median of the individual data. The lower and upper hinges represent the 25th and 75th percentiles. The upper and lower whiskers extend from the hinge to the largest or smallest measured values, respectively, but not more than 1.5 times the difference between the 25th and 75th percentiles. The mean is shown as grey points for the MP and grey triangles for the CP. Outliers are individual data points that fall outside of this range and are color-coded black.

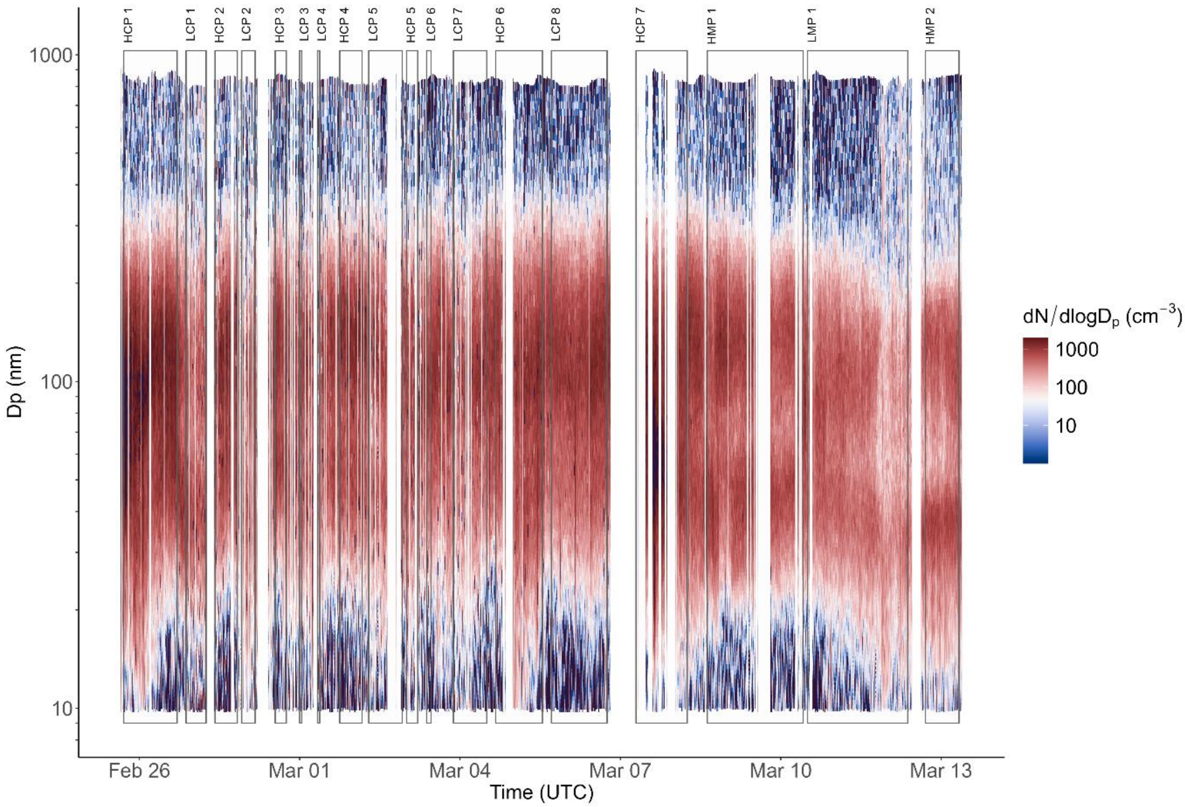

Figure S6: Aerosol number size distribution for the entire measurement period. The boxes represent periods where values deviate more than 10% from the median of the CN concentration. Periods with values more than 10% higher than the median are labelled high continental period (HCP 1-7) or high marine period (HMP 1-2), those with values more than 10% lower than the median low continental period (LCP 1-8) or low marine period (LMP 1).

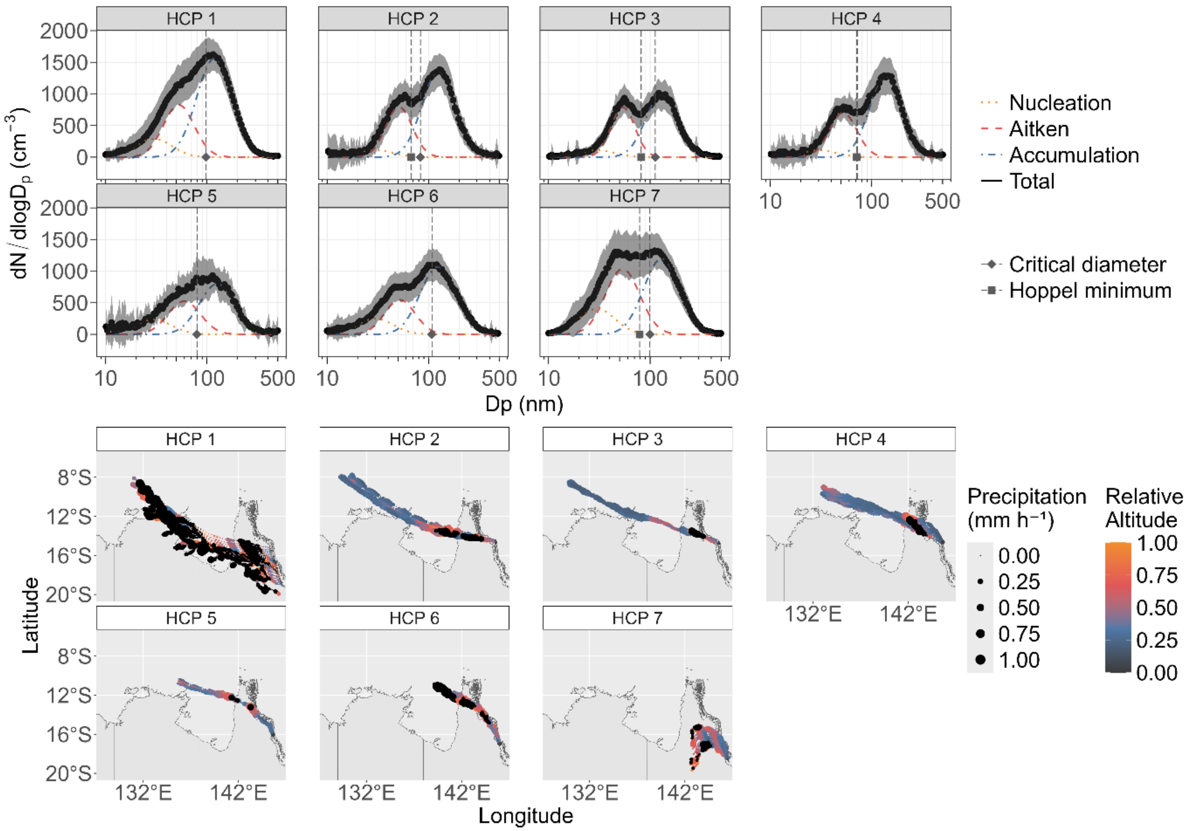

Figure S7: Average aerosol number size distributions (top) and the three-day back-trajectories (bottom) for the seven continental high CN number concentration periods (HCP1-7). The lines in the size distribution plots represent lognormal fits for the nucleation mode (dotted orange), Aitken mode (dashed red), accumulation mode (dot-dashed blue), and total (solid black). The dashed grey vertical line at the diamond-shaped point represents the critical diameter (D_{crit}), whereas the dashed grey vertical line at the square-shaped point represents the Hoppel minimum. Back-trajectories are coloured by their altitude in respect to the planetary boundary layer height. Black data points represent air masses travelling through the free troposphere. The precipitation amount determines the size of the trajectory points. The ship location marks the start point of each trajectory. The GBR was provided in the gisaimsr package by the Geoscience

Australia (GA) and the Great Barrier Reef Marine Park Authority (GBRMPA). The continental boundaries were obtained from the ozmaps package (doi:10.32614/CRAN.package.ozmaps).

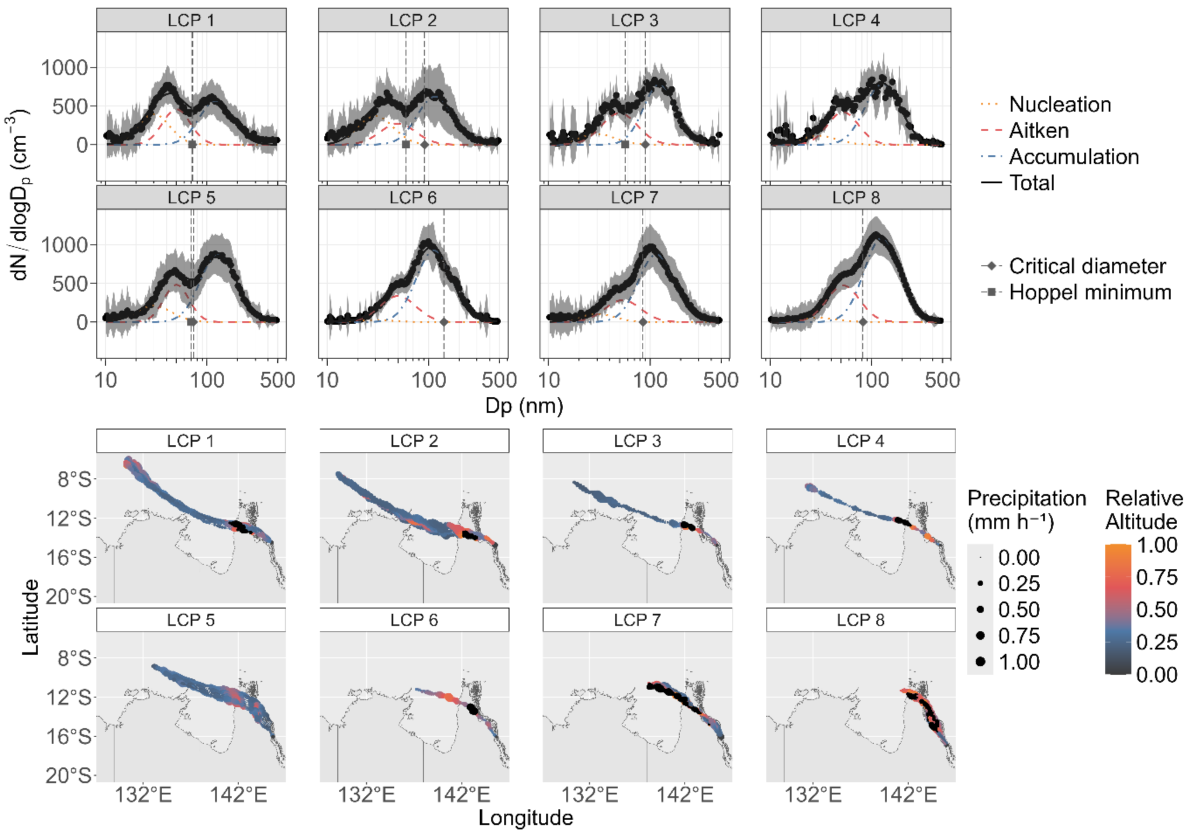

Figure S8: Average aerosol number size distributions (top) and the three-day back-trajectories (bottom) for the eight continental low CN number concentration periods (LCP1-8). The lines in the size distribution plots represent lognormal fits for the nucleation mode (dotted orange), Aitken mode (dashed red), accumulation mode (dot-dashed blue), and total (solid black). The dashed grey vertical line at the diamond-shaped point represents the critical diameter (D_{crit}), whereas the dashed grey vertical line at the square-shaped point represents the Hoppel minimum. No CCN data for 0.3% SS were available during LCP4. Back-trajectories are coloured by their altitude in respect to the planetary boundary layer height. Black data points represent air masses travelling through the free troposphere. The precipitation amount determines the size of the trajectory points. The ship location marks the start point of each trajectory. The GBR was provided in the gisaimsr package by the Geoscience Australia (GA) and the Great Barrier Reef Marine Park Authority (GBRMPA). The continental boundaries were obtained from the ozmaps package (doi:10.32614/CRAN.package.ozmaps).

Figure S9: Spearman correlation coefficient ($p < 0.05$) between CCN number concentration, CN number concentration inferred from the total fit, number concentration in the accumulation mode, number concentration in the Aitken mode, number concentration in the nucleation mode, averaged precipitation along one trajectory, and the percentage of time the trajectory spent in the FT for the seven continental high CN number concentration periods (HCP1-7).

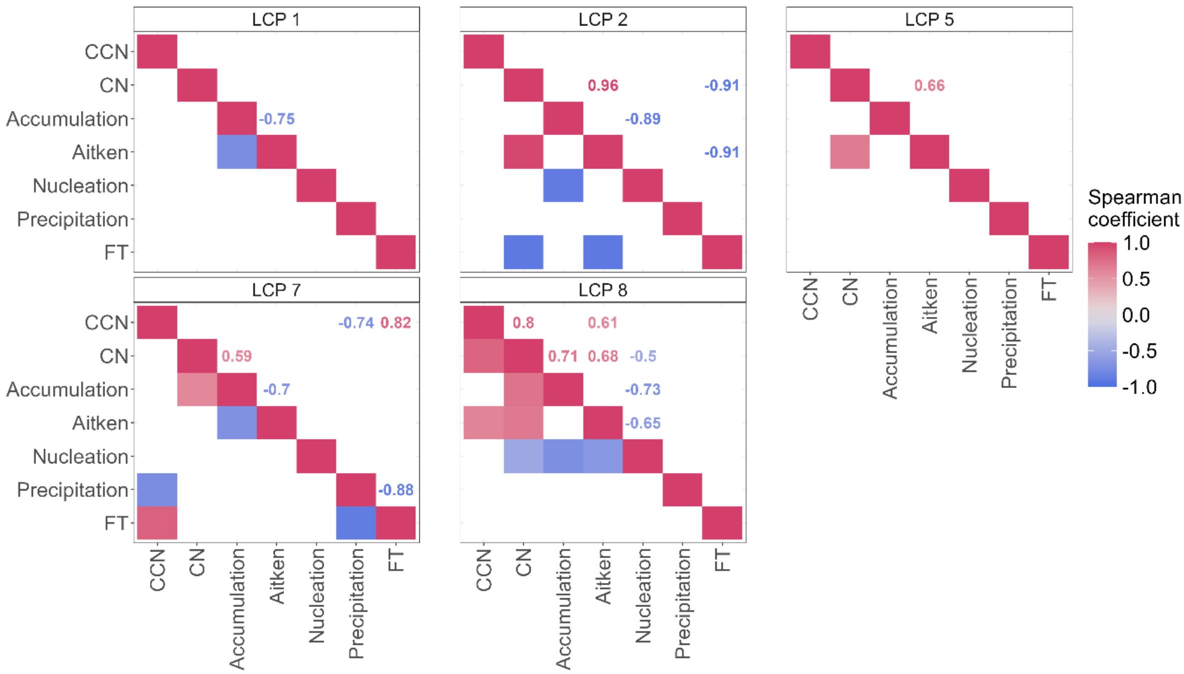

Figure S10: Spearman correlation coefficient ($p < 0.05$) between CCN number concentration, CN number concentration inferred from the total fit, number concentration in the accumulation mode, number concentration in the Aitken mode, number concentration in the nucleation mode, averaged precipitation along one trajectory, and the percentage of time the trajectory spent in the FT for five continental low CN number concentration periods (LCP1-2, LCP5, LCP7-8). LCP3-4, and LCP6 do not include enough data points to perform a correlation analysis.

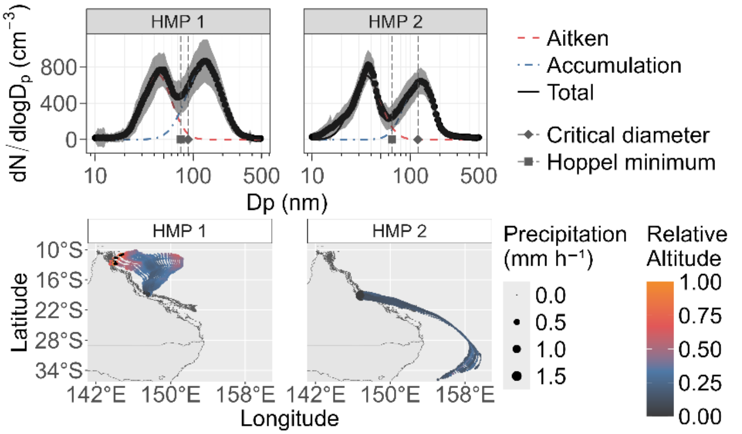

Figure S11: Average aerosol number size distributions (top) and the three-day back-trajectories (bottom) for the two marine high CN number concentration periods (HMP1-2). The lines in the size distribution plots represent lognormal fits for the nucleation mode (dotted orange), Aitken mode (dashed red), accumulation mode (dot-dashed blue), and total (solid black). The dashed grey vertical line at the diamond-shaped point represents the critical diameter (D_{crit}), whereas the dashed grey vertical line at the square-shaped point represents the Hoppel minimum. Back-trajectories are coloured by their altitude in respect to the planetary boundary layer height. Black data points represent air masses travelling through the free troposphere. The precipitation amount determines the size of the trajectory points. The ship location marks the start point of each trajectory. The GBR was provided in the gisaimsr package by the Geoscience Australia (GA) and the Great Barrier Reef Marine Park Authority (GBRMPA). The continental boundaries were obtained from the ozmaps package (doi:10.32614/CRAN.package.ozmaps).

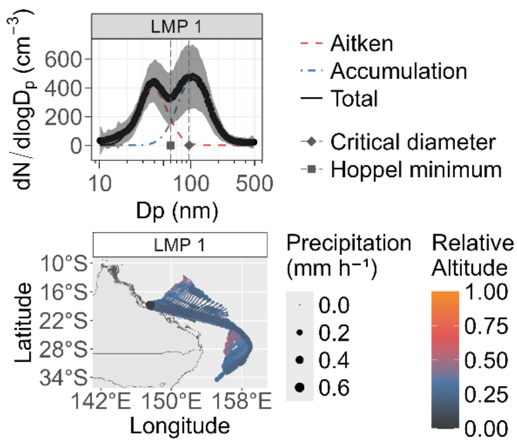

Figure S12: Average aerosol number size distributions (top) and the three-day back-trajectories (bottom) for the marine low CN number concentration periods (LMP1). The lines in the size distribution plots represent lognormal fits for the nucleation mode (dotted orange), Aitken mode (dashed red), accumulation mode (dot-dashed blue), and total (solid black). The dashed grey vertical line at the diamond-shaped point represents the critical diameter (D_{crit}), whereas the dashed grey vertical line at the square-shaped point represents the Hoppel minimum. Back-trajectories are coloured by their altitude in respect to the planetary boundary layer height. Black data points represent air masses travelling through the free troposphere. The precipitation amount determines the size of the trajectory points. The ship location marks the start point of each trajectory. The GBR was provided in the gisaimsr package by the Geoscience Australia (GA) and the Great Barrier Reef Marine Park Authority (GBRMPA). The continental boundaries were obtained from the ozmaps package (doi:10.32614/CRAN.package.ozmaps).

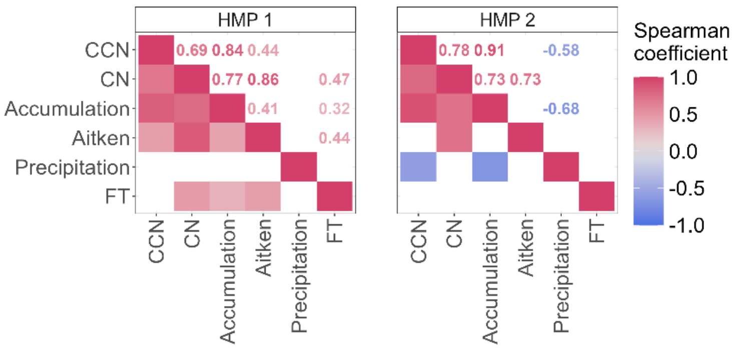

Figure S13: Spearman correlation coefficient ($p < 0.05$) between CCN number concentration, CN number concentration inferred from the total fit, number concentration in the accumulation mode, number concentration in the Aitken mode, number concentration in the nucleation mode, averaged precipitation along one trajectory, and the percentage of time the trajectory spent in the FT for the two marine high CN number concentration periods (HMP1-2).

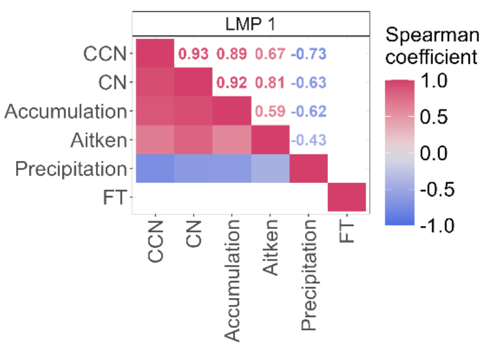

Figure S14: Spearman correlation coefficient ($p < 0.05$) between CCN number concentration, CN number concentration inferred from the total fit, number concentration in the accumulation mode, number concentration in the Aitken mode, number concentration in the nucleation mode, averaged precipitation along one trajectory, and the percentage of time the trajectory spent in the FT for the marine low CN number concentration periods (LMP1).

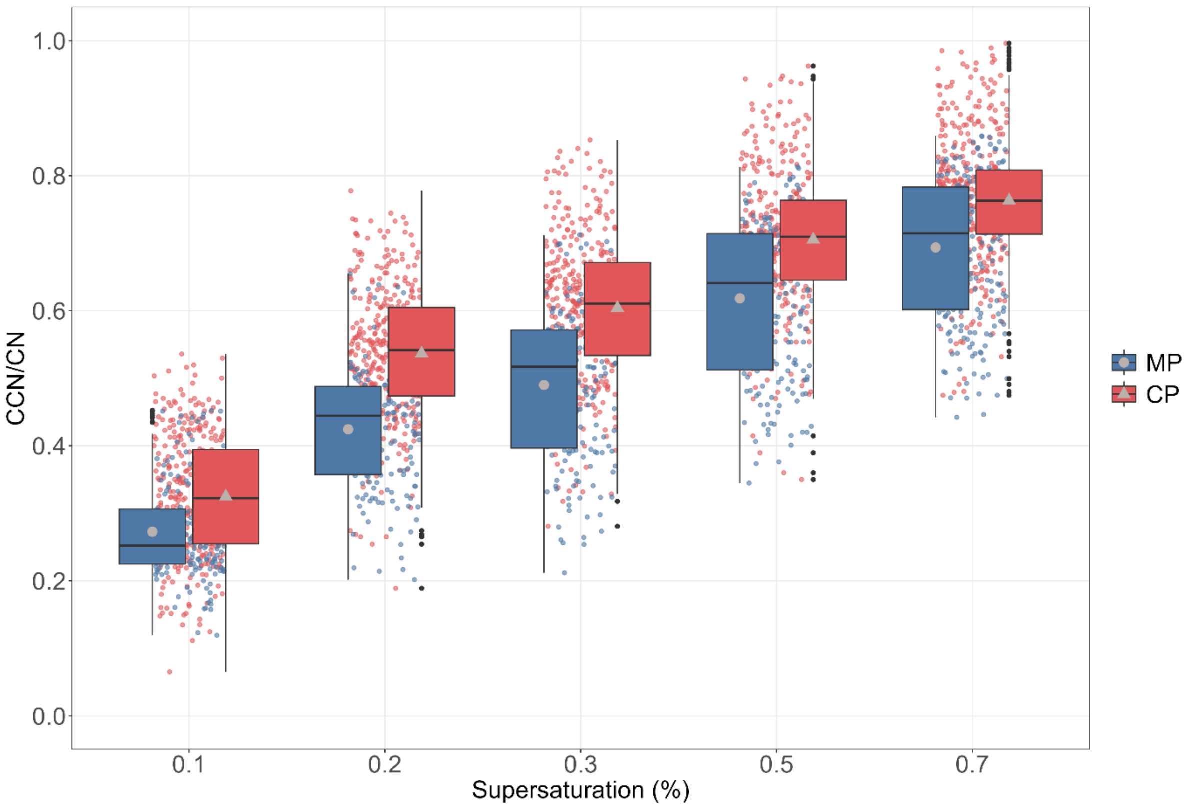

Figure S15: CCN activation ratios CCN/CN for the MP (blue) and CP (red) averaged on a minute timeframe at different supersaturations. The black horizontal line in a box displays the median of the individual data. The lower and upper hinges represent the 25th and 75th percentiles. The upper and lower whiskers extend from the hinge to the largest or smallest measured values, respectively, but not more than 1.5 times the difference between the 25th and 75th percentiles. The mean is shown as grey points for the MP and grey triangles for the CP. Outliers are individual data points that fall outside of this range and are color-coded black.

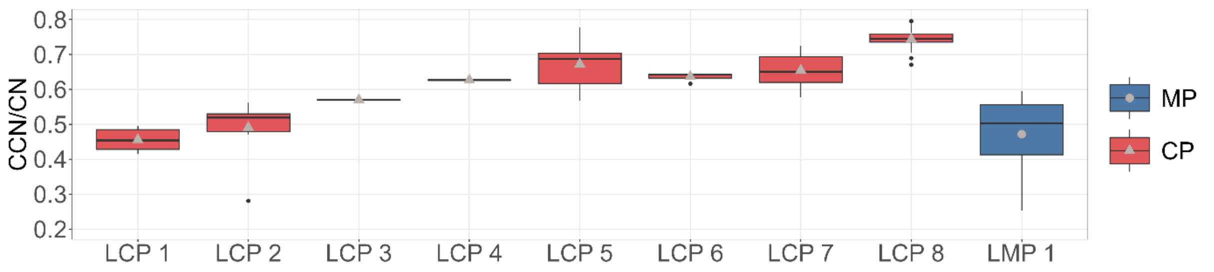

Figure S16: CCN activation ratios (CCN/CN) at 0.3 % SS for the MP (blue) and the CP (red) for the low CN number concentration periods (LCP1-8 and LMP1). The black horizontal line in a box displays the median of the individual data. The lower and upper hinges represent the 25^{th} and 75^{th} percentiles. The upper and lower whiskers extend from the hinge to the largest or smallest measured values, respectively, but not more than 1.5 times the difference between the 25^{th} and 75^{th} percentiles. The mean is shown as grey points for the MP and grey triangles for the CP. Outliers are individual data points that fall outside of this range and are color-coded black.

Table S1: Critical diameter (D_{crit}) and Hoppel minimum

	Critical diameter (D_{crit}) (nm)	Hoppel minimum (nm)
CP	99.00	(66.1)
MP	96.00	68.3
HCP1	97.79	/
HCP2	83.24	67.1
HCP3	112.43	81.8
HCP4	72.21	71.1
HCP5	79.75	/
HCP6	107.89	/
HCP7	99.33	78.8
LCP1	72.45	71.7
LCP2	91.47	60.0
LCP3	89.73	56.6
LCP4	/	/
LCP5	73.76	69.6
LCP6	141.95	/
LCP7	85.04	/
LCP8	82.01	/
HMP1	89.01	74.9
HMP2	119.82	65.3
LMP1	94.50	59.8

References

1 Beddows, D. C. S., Dall'Osto, M., and Harrison, R. M.: An Enhanced Procedure for the Merging of Atmospheric Particle Size Distribution Data Measured Using Electrical Mobility and Time-of-Flight Analysers, Aerosol Sci. Technol., 44:11, 930-938, doi:10.1080/02786826.2010.502159, 2010.

2 Conrad, B. M. and Johnson, M. R.: Mass absorption cross-section of flare-generated black carbon: Variability, predictive model, and implications. Carbon, 149, 760-771, doi:10.1016/j.carbon.2019.04.086, 2019.

3 DeCarlo, P. F., Slowik, J. G., Worsnop, D. R., Davidovits, P., and Jimenez, J. L.: Particle Morphology and Density Characterization by Combined Mobility and Aerodynamic Diameter Measurements. Part 1: Theory, Aerosol Sci. Technol., 38, 1185–1205, doi:10.1080/027868290903907, 2004.

4 Draxler, R. R., and Rolph, G. D.: HYbrid Single-Particle Lagrangian Integrated Trajectory Model, In: National Air Quality Conference, NOAA Air Resource Laboratory, https://www.arl.noaa.gov/documents/workshop/NAQC2007/HTML_Docs/index.html, 2007.

5 Gong, X., Wang, Y., Xie, H., Zhang, J., Lu, Z., Wood, R., Stratmann, F., Wex, H., Liu, X., and Wang, J.: Maximum supersaturation in the marine boundary layer clouds over the North Atlantic, AGU Advances, 4, e2022AV000855, doi.:10.1029/2022AV000855, 2023.

6 Heintzenberg, J., Covert, D., and Van Dingenen, R.: Size distribution and chemical composition of marine aerosols: a compilation and review, Tellus B: Chem. Phys. Meteorol., 52, 1104–1122, doi:10.3402/tellusb.v52i4.17090, 2000.

7 Laing, J. R., Jaffe, D. A., and Sedlacek III, A. J.: Comparison of Filter-based Absorption Measurements of Biomass Burning Aerosol and Background Aerosol at the Mt. Bachelor Observatory. Aerosol Air Qual. Res., 20, 663-678, doi:10.4209/aaqr.2019.06.0928, 2020.

8 Petters, M. D., and Kreidenweis, S. M.: A single parameter representation of hygroscopic growth and cloud condensation nucleus activity, Atmos. Chem. Phys., 7, 1961-1971, doi:10.5194/acp-7-1961-2007, 2007.

9 Stein, A. F., Draxler, R. R., Rolph, G. D., Stunder, B. J., Cohen, M. D., and Ngan, F.: NOAA's HYSPLIT Atmospheric Transport and Dispersion Modeling System, B. Am. Meteorol. Soc., 96, 2059-2077, doi:10.1175/bams-d-14-00110.1, 2015.

10 Wexler, A. S. and Clegg, S. L.: Atmospheric aerosol models for systems including the ions H^+, NH_4^+, Na^+, SO_4^{2-}, NO^{3-}, Cl^-, Br^-, and H_2O, J. Geophys. Res., 107(D14), 4207, doi:10.1029/2001JD000451, 2002.